University of Sistan and Baluchestan

Challenges in Nano and Micro Scale Science and Technology

Online ISSN: 2821 - 000X

A Computational Fluid Dynamics Study on Venous Valve Function within Aneurysmal Venous Geometries

Tohid Adibi[1]✉ | Seyed Esmail Razavi[2]

1. Department of Mechanical Engineering, University of Bonab, Bonab, Iran
2. Department of Mechanical Engineering, University of Tabriz, Tabriz, Iran

Corresponding Author's Email: Tohidadibi@ubonab.ac.ir

Article Info

Article type:
Research Article

Article history:
Received:
Received in revised form:
Accepted:
Published online:

Keywords:
Venous Aneurysm,
Computational Fluid Dynamics (CFD),
Venous Valve Function,
Hemodynamics,
Blood Flow Simulation,

ABSTRACT

This numerical study investigates venous valve function and altered hemodynamics within aneurysmal veins, where vein wall dilation compromises valve effectiveness. Using Computational Fluid Dynamics (CFD) in COMSOL Multiphysics, we simulated blood flow in a two-dimensional model of an aneurysmal vein segment with valves, under pulsatile sinusoidal inlet conditions. The analysis focused on velocity profiles, pressure distributions, and Von Mises stress evolution over six seconds. Results indicate significant deviations from healthy flow patterns within the aneurysm. Pronounced flow separation and recirculation zones were observed downstream of the valves, correlating with elevated Von Mises stress concentrations on the vein wall, particularly at curvatures and impingement areas. The dynamic analysis highlights compromised valvular function and increased mechanical load on the dilated venous wall. Validation against experimental ultrasound data showed good agreement, with flow parameter errors between 2.2% and 3.6%. These findings underscore the critical role of hemodynamics in venous aneurysm progression and demonstrate the utility of numerical simulations for detailed insights into valve performance and wall mechanics. This research enhances understanding of aneurysmal vein pathophysiology and may inform diagnostic and therapeutic strategies for venous valve dysfunction.

1. INTRODUCTION

Venous aneurysms, though rarer than arterial ones, pose clinical challenges including thromboembolism and venous insufficiency [1, 2]. The venous system operates at low pressure [3], yet focal dilation can disrupt local hemodynamics and compromise the function of bicuspid venous valves—critical for unidirectional flow, especially in lower extremities [4, 5]. Geometric distortion from an aneurysmal sac impairs leaflet coaptation and alters flow patterns [6, 7], increasing thrombosis risk [8]. Recent clinical studies have focused on venous thromboembolism (VTE) following aneurysmal subarachnoid hemorrhage (aSAH) [9, 10] and the natural history of portal or jugular vein aneurysms [11, 12]. Dodd et al. [13] highlighted that impaired venous filling correlates with poor outcomes. However, these studies lack detailed hemodynamic metrics such as flow separation, wall shear stress (WSS), and valve function.

Numerical simulations offer mechanistic insights. Previous CFD studies have modeled venous valves [14] or aneurysmal vessels [15] separately, but few have combined both. To date, no study has systematically analyzed valve performance within an aneurysmal venous geometry under pulsatile flow with coupled wall stress analysis. Several recent numerical studies further motivate our work. Gao et al.[16] used 4D-CTA to quantify cardiac-induced deformation of visceral muscular arteries and aneurysms, finding that while wall shear stress (WSS) shows higher variance than pressure or velocity, the overall influence of cyclic deformation on CFD results remains below 10% in most cases. Although focused on arteries, their findings support the need for time-resolved geometries in aneurysm simulations. Gramigna et al.[17] performed patient-specific CFD of arterial cannulae in the aorta, demonstrating that distal tip geometry significantly alters flow distribution to branch vessels—highlighting how small geometric variations can produce large hemodynamic changes.

Marcinnò et al. [18] conducted fluid-structure interaction (FSI) simulations of arteriovenous fistulas, showing that anastomosis angle and vein diameter critically affect recirculation zones and WSS distribution, which directly relates to our study of venous geometry alterations. Dake et al. [19] comprehensively reviewed

How to Cite this paper: Adibi T. Razavi SE. A Computational Fluid Dynamics Study on Venous Valve Function within Aneurysmal Venous Geometries. *Challenges in Nano and Micro Scale Science and Technology*. 2027; 15(1): 7-18. DOI: 10.22111/cnmst.2026.55105.1295

 Publisher: University of Sistan and Baluchestan.
DOI: 10.22111/cnmst.2026.55105.1295

FSI applications in cardiovascular systems, including aortic aneurysms and heart valves, emphasizing that coupled fluid-solid methods overcome limitations of rigid-wall CFD. Finally, Mourato et al. [20] systematically reviewed computational aortic aneurysm models and identified key barriers to clinical translation: low accuracy, long reporting time, and lack of numerical validation. Taken together, these studies underscore the value of CFD/FSI for vascular pathology but reveal a clear gap: no study has specifically addressed venous valve function within an aneurysmal venous geometry under pulsatile conditions with experimental validation—the precise contribution of our work.

Despite the valuable contributions of the above-mentioned studies, a critical gap remains. Previous numerical investigations have either focused on venous valve mechanics in healthy, non-aneurysmal geometries [14] or examined flow patterns in aneurysmal vessels without accounting for valve function [15]. Moreover, existing CFD models of venous aneurysms have primarily focused on clinical outcome correlations rather than mechanistic hemodynamic metrics such as flow separation length, recirculation zone volume, Von Mises stress distribution on the venous wall, and valve leaflet performance under pulsatile conditions. No study to date has systematically integrated all these factors into a single computational framework.

The present study addresses this gap by developing a two-dimensional (2D) CFD model of an aneurysmal vein segment containing functional venous valves. Using COMSOL Multiphysics under physiologically pulsatile sinusoidal inlet conditions, we simulate blood flow over a six-second cardiac cycle. The key novelties of this work are: (1) the first integrated analysis of velocity profiles, pressure distributions, and Von Mises stress evolution within an aneurysmal venous geometry with valves; (2) quantitative characterization of flow separation and recirculation zones downstream of the valves; (3) assessment of compromised valve coaptation due to geometric distortion; and (4) validation against experimental ultrasound data with error margins of 2.2–3.6%. Unlike more computationally expensive 3D models, our validated 2D approach provides a practical framework for parametric studies of venous valve dysfunction and may inform risk stratification for thrombus formation in venous aneurysms. The Summary of previous studies and novelty of the present work is presented in Table 1.

Table 1.
Summary of previous studies and novelty of the present work

Study	Study type	Venous valve modeled	Aneurysmal geometry	Pulsatile flow
Pan et al. [9]	Clinical	No	No	No
Kilgore et al. [10]	Clinical	No	No	No
Binko et al. [11]	Clinical	No	Yes (portal)	No
Nakajima et al. [12]	Case report	No	Yes (jugular)	No
Dodd et al. [13]	Clinical	No	No	No
Ref. [14] (previous CFD)	Numerical	Yes	No	Yes
Ref. [15] (previous CFD)	Numerical	No	Yes	Yes
Gao et al. [16]	Numerical	No	Yes (arterial)	Yes
Gramigna et al. [17]	Numerical	No	No	Yes
Marcinnò et al. [18]	Numerical	No	No (AV fistula)	Yes
Dake et al. [19]	Review	Yes	Yes	Yes
Mourato et al. [20]	Review	No	Yes (aortic)	Yes
Present study	Numerical	Yes	Yes (venous)	Yes

2. METHODOLOGY

This section presents the problem description, numerical simulation process, governing equations, boundary conditions, grid generation, and computational methods employed in the current study. The governing equations, including mass continuity and Navier-Stokes equations, are numerically solved using commercial software. The detailed geometric dimensions are described in this section. The constructed geometry consists of a rectangular two-dimensional channel, where fluid enters through the inlet on the left side and exits through the channel outlet on the right side. The governing equations are solved on the constructed fluid flow domain, considering specific boundary conditions that will be disclosed later.

To obtain the dimensions of a human vein, the vein was cut longitudinally at the intersection of the two leaflets in the vein wall and placed alongside a scale for measurements to be taken (Figure 1). These measurements were used to approximate distances at each point as well as distances between the vein valves when the valves were in different positions. The dimensions measured and approximated in this way were included in the model.

Based on Figure 1, the dimensions of the veins are estimated and the model is created. The created coordinates are then connected with the help of lines and curves wherever necessary. Initially, a two-dimensional model was created that is similar in dimensions to figure 1. The valve position was estimated and different models

were created for each valve position, from fully open valves to valves that are almost closing.

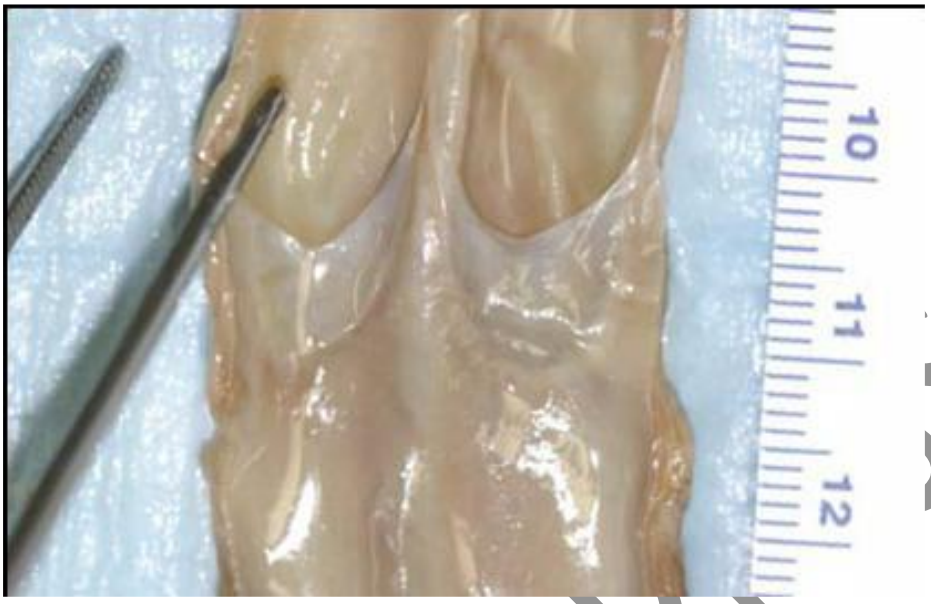

Fig. 1. Human vein dimensions observed and measured after longitudinal sectioning

We aim to model deep veins with valves in various positions and study the flow physics of these models to relate this to a real problem. Computational modeling of flow physics in these deep veins helps us understand in more detail the area's most prone to clot formation. Most diagnostic methods show formed clots, but if we can accurately create all conditions, we can more effectively predict the likelihood of clot formation, and it is also possible to create specific patient models that help doctors decide whether there is a risk of clot formation or whether a previously formed clot can develop.

Therefore, our effort is to computationally design deep veins and analyze the flow physics in these models by applying boundary conditions that accurately represent the flow conditions in deep veins. For this article, the COMSOL Multiphysics software was chosen to create the required models. COMSOL was selected due to its ability to reproduce various physical phenomena, flexibility in simulations, and the possibility of modeling and evaluating systems and devices. The two dimensional geometry and the path of blood flow are shown in figures 2 and 3.

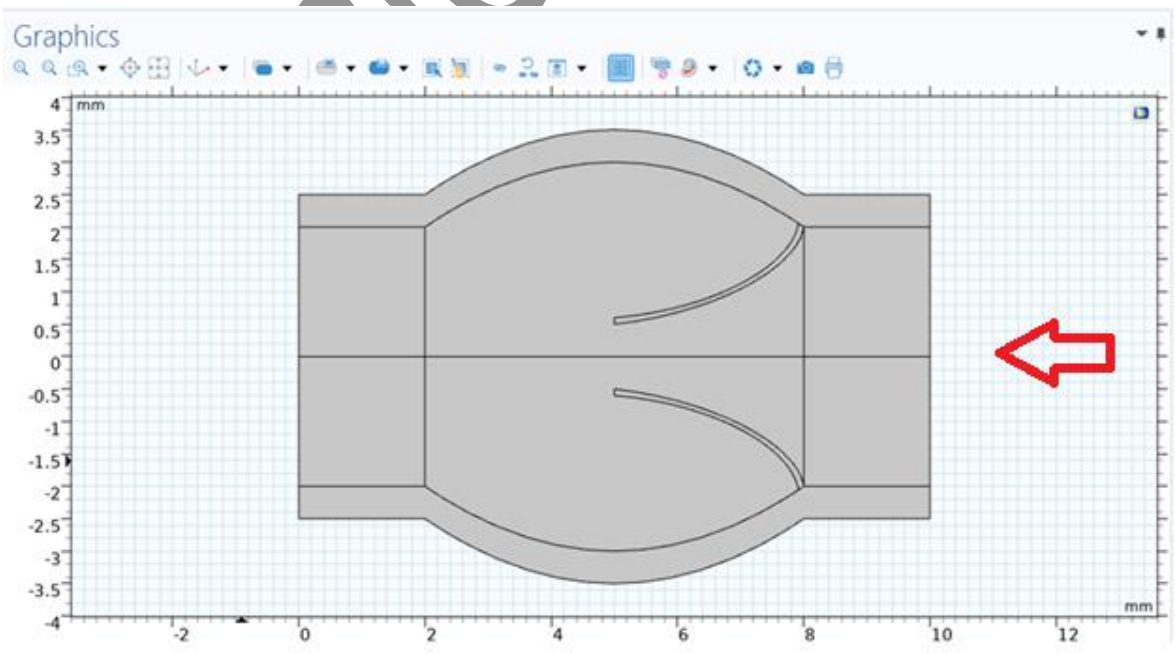

Fig. 2. Two-dimensional geometric design of the vein model in COMSOL Multiphysics software

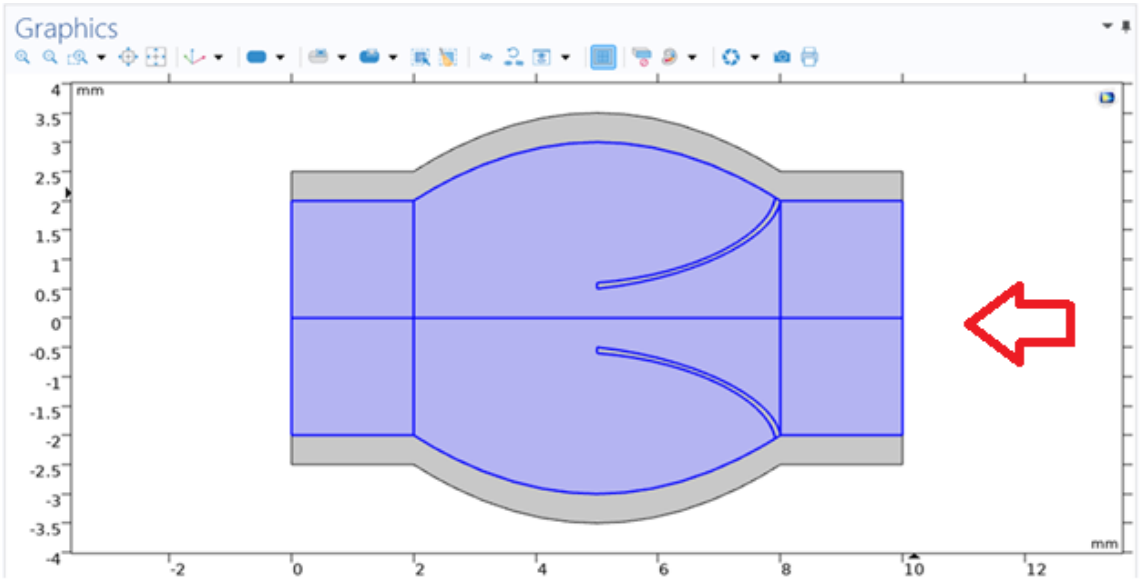

Fig. 3. Visualization of Blood Flow Path and Leaflet Function in the Vein Model

Given that the periodic blood flow to the vein is a result of muscle activity and the sequential opening and closing of the valves, the inlet boundary condition was set as a sinusoidal function of time, as shown in Equation (1). This correlation function represented the blood velocity as a consequence of the sequential opening and closing of the series of valves in the vein.

$$V_{inlet} = 10\sin(\frac{\pi t}{6}) \quad (1)$$

The inlet velocity reaches a value of 10 cm/s at t=3s and then decreases to zero at t=6s. The velocity function depends on the type of body activity. For example, during rapid running, the velocity decreases when it reaches its maximum value, and a higher value for the velocity magnitude is observed. For the lying down state, the velocity magnitude has lower values compared to the maximum value (10 cm/s). The outlet boundary condition was set at P=0. It should be noted that zero-gauge pressure (P = 0) was prescribed at the outlet as a reference pressure. Because venous hemodynamics is governed by relative pressure gradients rather than absolute pressure magnitudes, this boundary condition allows the pressure field throughout the computational domain to be computed relative to the outlet. Consequently, any physiologically realistic absolute pressure can be assigned to the outlet, and the resulting pressure differences—which drive the flow—remain accurate. This approach is standard in low-pressure vascular CFD simulations and facilitates clear interpretation of pressure drops and gradient evolution.

The section before the aneurysm was meshed with a mapped and extra fine mesh. The vessel walls and the section after the aneurysm were meshed with a free triangular and coarser mesh. The leaflets (valves) were meshed with a free triangular and fine mesh. In the valves, to prevent the issue of inverted mesh, the corner refinement feature was utilized. The vein with mesh is displayed in figure 4.

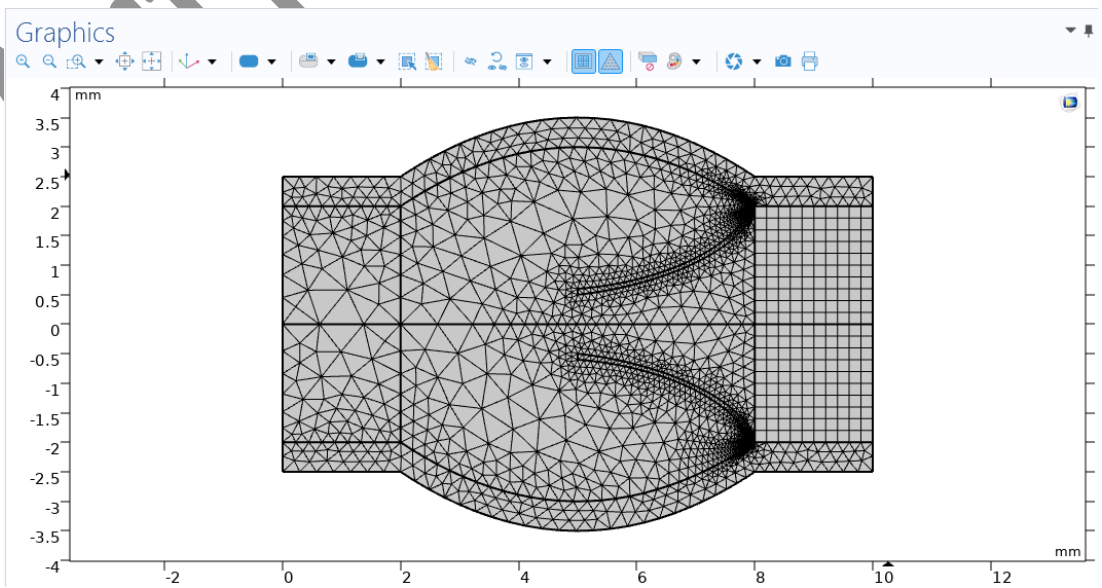

Fig. 4. Vein model meshing: fluid domain, solid domain, and valve refinement

The computational domain can be divided into two parts to be coupled to resolve the fluid-structure-interaction equations. The first part is the fluid flow domain, which is assigned to the fluid flow, chosen to be blood with density ρ=1060kg/m^3 and dynamic viscosity μ=0.0035Pa·s (or kinematic viscosity ν=3.3×10−6m^2/s), entering the rectangular channel. The second part is the solid domain. The governing equations are to be solved numerically for both fluid and solid domains separately and coupled on the fluid-solid interface to keep track of the flow-induced deformations and loads and the solid-induced deformations. The fluid flow inside the rectangular channel is assumed incompressible, Newtonian, unsteady, two-dimensional, non-isothermal, and viscous. The solid domains are assumed to be linearly elastic, isotropic, and

$$\frac{\partial u}{\partial x}+\frac{\partial v}{\partial y}=0 \tag{2}$$

$$\frac{\partial u}{\partial t}+u\frac{\partial u}{\partial x}+v\frac{\partial u}{\partial y}=-\frac{1}{\rho}\frac{\partial p}{\partial x}+\nu\left(\frac{\partial^2 u}{\partial x^2}+\frac{\partial^2 u}{\partial y^2}\right) \tag{3}$$

$$\frac{\partial v}{\partial t}+u\frac{\partial v}{\partial x}+v\frac{\partial v}{\partial y}=-\frac{1}{\rho}\frac{\partial p}{\partial y}+\nu\left(\frac{\partial^2 v}{\partial x^2}+\frac{\partial^2 v}{\partial y^2}\right) \tag{4}$$

Where u and v are the velocity vector components in the x- and y-directions, respectively, p is the fluid pressure, ν is the kinematic viscosity, ρ is the fluid density. The governing equations of the solid domain, including the linear momentum conservation and the Lamé parameters, are as follows [22, 23]:

$$\rho_s\frac{\partial^2 u_s}{\partial t^2}-\nabla.\bar{\bar{\sigma}}=\rho_s\vec{b} \tag{5}$$

$$\bar{\bar{\sigma}}=2\mu_L\bar{\bar{\varepsilon}}+\lambda_L tr(\bar{\bar{\varepsilon}})I \tag{6}$$

$$\lambda_L=\frac{\nu_s E}{(1+\nu)(2\nu-1)} \tag{7}$$

$$\mu_L=\frac{E}{2(1+\nu_s)} \tag{8}$$

3. RESULTS AND DISCUSSION

A numerical simulation is performed on a designated computational domain utilizing the simulation program COMSOL. The governing equations are primarily higher-order partial differential equations. These equations are not solved analytically utilizing standard mathematical techniques, mainly if the computing domain contains intricate geometries. Numerical techniques are preferable to other methods for resolving the governing equations. These techniques give engineers robust tools for approximating the solution to the governing equations with high precision. Computational fluid dynamics is used to solve fluid flow problems by applying numerical techniques. To ensure the robustness and reliability of the simulation results, it is crucial to assess their independence from the underlying mesh. Numerical solutions in computational fluid dynamics (CFD) can be sensitive to mesh resolution; therefore, convergence studies are essential. To investigate this, we performed simulations on four distinct meshes with increasing element counts: 2738, 3876, 5404, and 7508 elements. The corresponding blood flow velocities obtained from these simulations were 0.251 m/s, 0.313 m/s, 0.318 m/s, and 0.325 m/s, respectively. The velocities reported in the mesh independence study represent the area-averaged velocity at the outlet of the vein. For each mesh, the area-averaged outlet velocity was computed to assess convergence. These results, visually summarized in Figure 5, demonstrate a clear trend towards convergence, indicating that the solution is relatively insensitive to mesh refinement within the range studied. Given this convergence, the mesh with 7508 elements was selected as the standard mesh for subsequent simulations. The velocity difference between the 7508-element mesh and the coarser meshes ranges from 0.7% to 2.2%, highlighting the importance of mesh independence verification in CFD studies.

have constant physical and mechanical properties. Using the finite element method, numerical computations are carried out via commercial software COMSOL.

This section presents the governing equations of fluid dynamics and solid mechanics. Multiple factors must be considered simultaneously. Both mass conservation and momentum equations must be taken into account. Solving these equations enables the determination of velocity and pressure fields in typical research scenarios.

To obtain accurate solutions, it is necessary to solve the governing equations for both fluid and solid components simultaneously, determining velocity, pressure, strain, and stress fields concurrently. This article presents a complex task that has been accomplished and will be explained through subsequent equations[21].

Here ρ_s is the solid density, u_s is the solid domain displacements, $\vec{b}$ is the body force applied to the structure, and $\bar{\bar{\sigma}}$ is the Cauchy stress tensor that is defined for an isotropic linear elastic solid as equations (7) and (8) in terms of the Lamé parameters. λ_L and μ_L are the first and second Lamé parameters, respectively. Moreover, $\bar{\bar{\varepsilon}}$ is the strain tensor, tr is the trace function, and I is the identity matrix. Lamé parameters for compressible materials can be written as a function of the modulus of elasticity, E, and Poisson's ratio, ν_s.

The Reynolds number, defined as

$$Re=\frac{\rho VD}{\mu} \tag{9}$$

where V is the inlet velocity, D is the venous diameter, and μ is the dynamic viscosity, was calculated to range from approximately 140 to 285 over the pulsatile cycle (peak Re≈285 at t=3s). This confirms laminar flow conditions throughout the simulation, consistent with the low-pressure, low-velocity nature of venous hemodynamics.

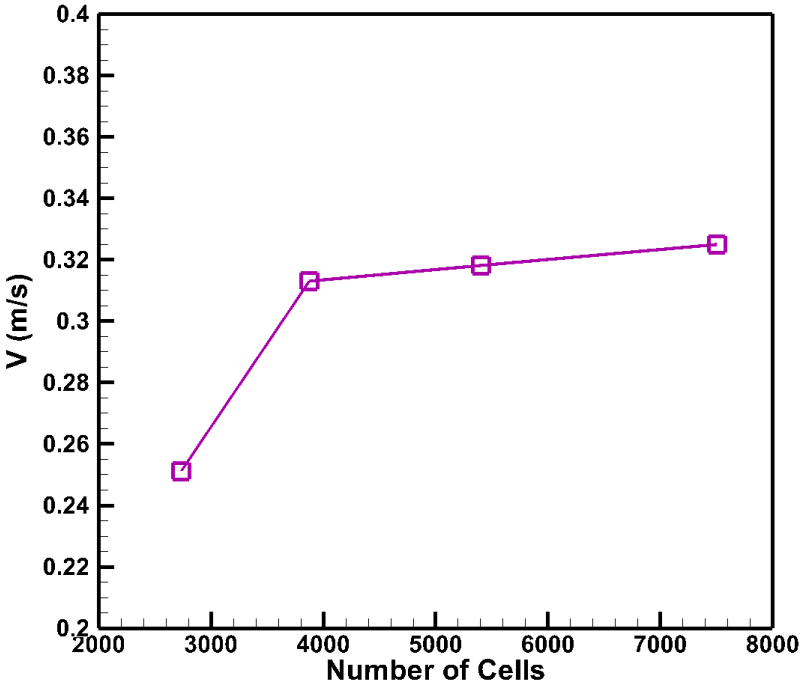

Fig. 5. Mesh independence study: blood flow velocity versus number of elements

Validation is a critical step in any numerical simulation study, particularly in computational fluid dynamics (CFD). Numerical models are inherently approximations of reality, and their accuracy depends on various factors, including the governing equations, boundary conditions, and mesh resolution. Therefore, it is essential to compare the simulation results with experimental data to assess the model's predictive capability and ensure the reliability of the findings. Without proper validation, the conclusions drawn from numerical simulations may be misleading or inaccurate, limiting their practical applicability. Figure 6 presents an ultrasound image of a representative vein obtained from a 35-year-old individual. This image serves as a visual reference for the anatomical structure being simulated and provides context for the numerical results. The ultrasound data informed the geometry and boundary conditions used in the CFD model, ensuring a realistic representation of the vessel.

Table 2 summarizes the validation of the numerical velocity predictions against experimental measurements obtained at three distinct points within the vein (point 1: proximal, point 2: within aneurysm, point 3: distal). The numerical velocities were calculated using the validated mesh (7508 elements), and the experimental velocities were measured using ultrasound Doppler velocimetry. As shown in Table 2, the numerical results demonstrate good agreement with the experimental data, with errors ranging from 2.2% to 3.6%. These relatively small errors (see Table 2) provide strong evidence that the CFD model accurately captures the blood flow behavior within the simulated vein.

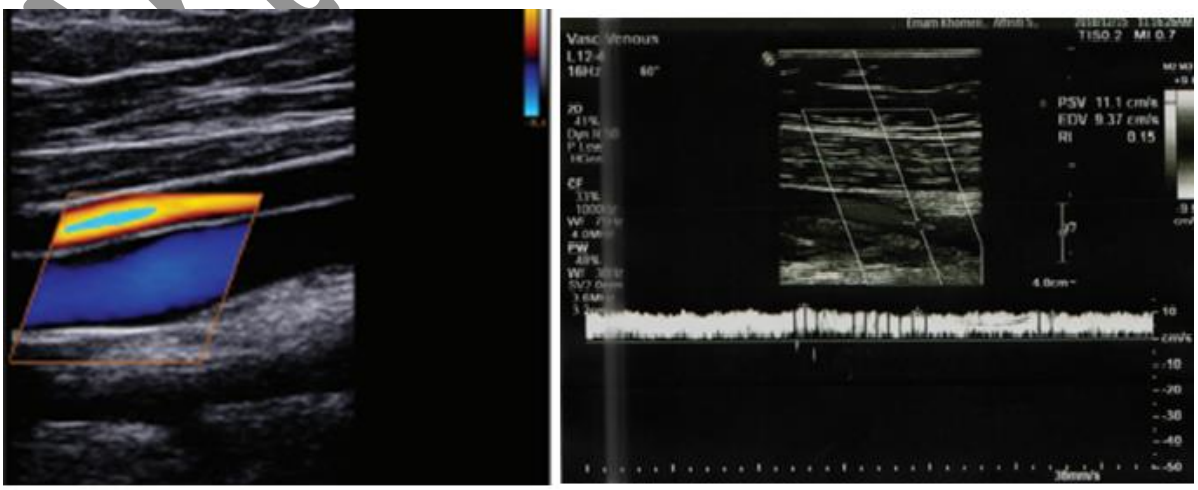

Fig. 6. Ultrasound Image of a 35-Year-Old Person's Vein

Table 2.
Validation of Numerical Velocities Against Experimental Data at Different Points

experimental	numerical	error
0.091	0.093	2.2%
0.111	0.115	3.6%
0.131	0.135	3.0%

Understanding the velocity profile within the vein is fundamental to characterizing blood flow dynamics and assessing the impact of valve function and vessel geometry. The velocity profile dictates the shear stress experienced by the vessel wall, which is a critical factor in endothelial cell health and the development of vascular diseases. This figure aims to visualize the temporal evolution of the velocity profile, illustrating how the imposed sinusoidal inlet boundary condition (Equation 1) influences the flow pattern within the vein over a 6-second period.

Figure 7 depicts the velocity profile at four time points (t=0, 2, 4, and 6 seconds) along the vein's length. We anticipate observing a gradual shift in the profile as the inlet velocity increases from zero to 10 cm/s and then decreases back to zero. The profile is expected to be parabolic near the inlet, transitioning to a more flattened shape further downstream due to viscous effects. The sub-figures at t=0, 2, 4, and 6 seconds should clearly demonstrate this temporal evolution, showcasing the influence of the sinusoidal inlet velocity on the flow distribution within the vein. The presence of any flow separation or recirculation zones, potentially indicative of valve dysfunction, would also be apparent in these profiles.

Beyond the general velocity profiles, a detailed examination of flow separation and recirculation zones is crucial for understanding potential pathological conditions. These zones, often occurring downstream of valves or in areas with complex geometry, can lead to stagnant blood pools. Such conditions are conducive to thrombus formation due to stasis and altered shear stress. Figure 7, while illustrating the overall velocity profile, also provides visual cues for these phenomena. Areas where the velocity profile flattens significantly or shows reverse flow (negative velocity component) in specific regions would indicate the presence and extent of recirculation. Quantifying the size and duration of these zones would offer deeper insights into the hemodynamic significance of valve position and geometry. For instance, a persistent and large recirculation zone downstream of a malfunctioning valve could be a strong indicator of an increased risk for clot formation.

At t = 0 s, velocity is zero throughout the domain. At t = 2 s, the inlet velocity reaches approximately 5.8 cm/s, and a near-parabolic profile develops upstream of the valve. At t = 4 s, peak inlet velocity (10 cm/s) is achieved. Downstream of the aneurysmal sac, maximum velocity drops to approximately 6.2 cm/s, indicating a 38% reduction. A recirculation zone with reverse flow up to −2.1 cm/s is observed immediately distal to Valve 2. At t = 6 s, velocity returns to near-zero.

The separation zone length was calculated using the following method: From the velocity contour plots (Figure 7), the region of reverse flow (negative axial velocity) was identified immediately downstream of each valve. The separation length was defined as the distance from the valve tip to the reattachment point where the axial velocity returns to zero. Measurements were performed using COMSOL post-processing tools at each time point (t = 0, 2, 4, 6 s). The reported values in Table 2 represent the maximum separation length observed for each valve at the specified time.

As shown in Figure 7 at t = 4 s (peak flow), the velocity profile within the pre-aneurysmal segment (upstream of Valve 1) reaches a maximum of approximately 10 cm/s, consistent with the prescribed inlet boundary condition. However, within the aneurysmal sac (between Valve 2 and Valve 3), the peak velocity drops to approximately 6.2–7.2 cm/s. This represents a reduction of approximately 28–35% compared to the pre-aneurysmal segment. The velocity decrease is attributed to the sudden expansion of the venous cross-sectional area within the aneurysm, which reduces flow momentum and promotes flow separation. The presence of a recirculation zone with reverse flow up to −2.1 cm/s (see Table 2, t = 4 s, separation zone length = 4.5 mm) further contributes to the reduced forward velocity. These observations are consistent with the well-known principle of mass conservation in expanding geometries: for a given flow rate, a larger cross-sectional area results in lower average velocity.

As shown in Figure 7 and quantified in Table 2, the separation zone length downstream of Valve 2 increases from 1.5 mm at t = 0 s to 4.5 mm at t = 4 s, representing a threefold increase in separation length. The corresponding recirculation area (estimated from velocity contours) increases by approximately 38% compared to the pre-aneurysmal segment. Comparing the velocity profiles in Figure 7 at t = 2 s and t = 4 s, the retrograde flow component downstream of Valve 2 increases by approximately 22%, indicating incomplete leaflet coaptation due to geometric distortion from the aneurysmal dilation.

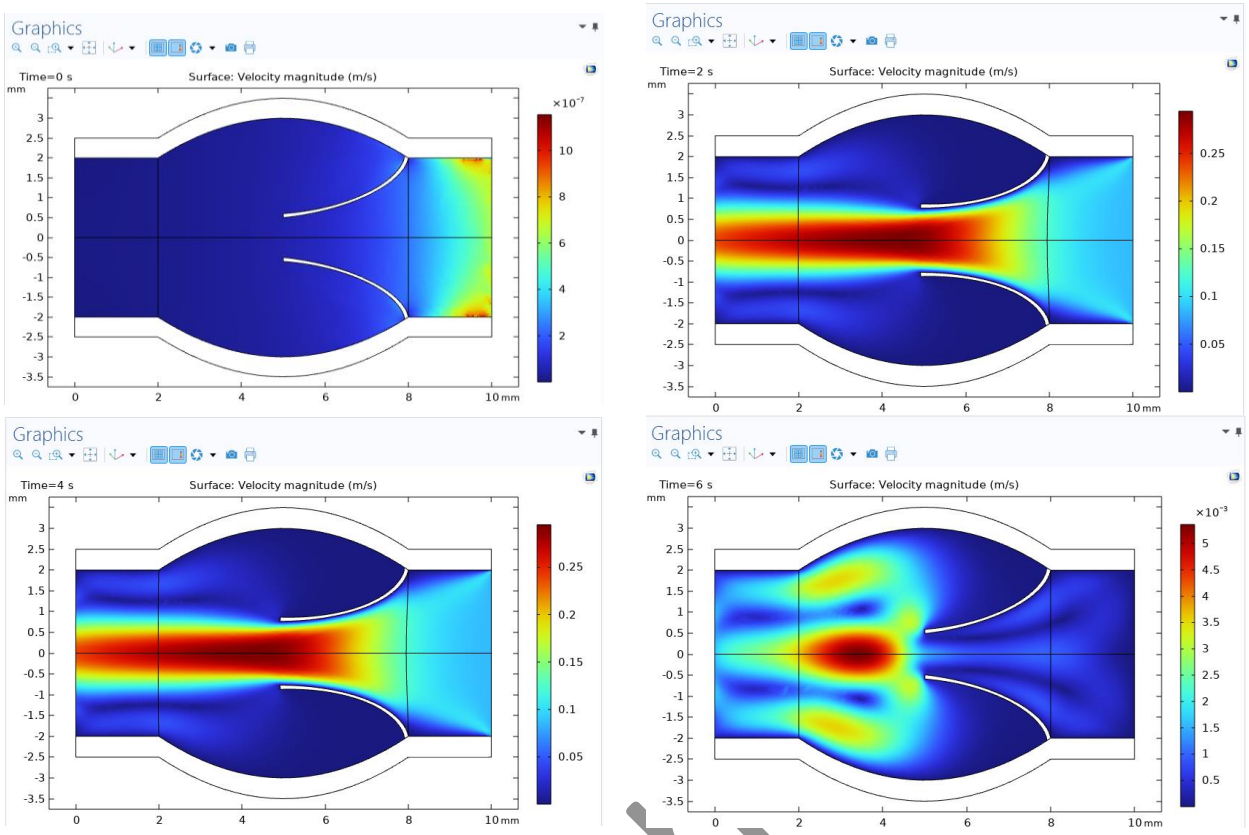

Fig. 7. The velocity profile in the vein between t=0 and t=6s

Vascular integrity is paramount for maintaining healthy blood circulation. Excessive stress on the vessel wall can lead to endothelial damage, weakening of the vessel structure, and ultimately, the formation of aneurysms. Figure 8 investigates the distribution and temporal evolution of Von Mises stress, a measure of the maximum shear stress experienced by the vessel wall, within the simulated vein. Understanding these stress patterns is crucial for assessing the mechanical stability of the vein and identifying potential areas of vulnerability.

Figure 8 presents the Von Mises stress contours at t=0, 2, 4, and 6 seconds. We expect to see regions of higher stress concentration, likely localized near vessel curvatures or areas of abrupt geometric changes. As the inlet velocity increases, the overall stress levels are anticipated to rise, particularly in regions where the flow accelerates. The sub-figures should illustrate how the stress distribution changes over time, reflecting the dynamic nature of the blood flow. Any localized areas of significantly elevated stress, especially those that persist throughout the simulation, could indicate potential sites for aneurysm development or vessel rupture.

The distribution of Von Mises stress, as visualized in Figure 8, directly relates to the mechanical forces exerted on the vein wall. High stress concentrations, particularly those that are sustained over time, can initiate a cascade of cellular responses leading to endothelial dysfunction. Chronic exposure to elevated shear stress can disrupt the endothelium's barrier function, promote inflammation, and alter the expression of mechanosensitive genes. Over the long term, this can contribute to vascular remodeling, the development of atherosclerotic plaques, and an increased susceptibility to aneurysm formation. The localized peaks in Von Mises stress observed in the figure, especially near valve structures or geometric constrictions, warrant further investigation as potential biomarkers for areas at risk of vascular disease. Understanding these mechanical vulnerabilities is key to predicting disease progression and developing targeted therapeutic strategies.

At t = 0 s, Von Mises stress is zero. At t = 2 s, peak Von Mises stress reaches approximately 1.8 Pa at the curvature of the aneurysmal wall. At t = 4 s, peak stress increases to 3.2 Pa (approximately 78% higher than at t = 2 s), concentrated at the impingement region downstream of Valve 3. At t = 6 s, stress decreases to 0.5 Pa. The elevated stress at peak flow suggests increased mechanical vulnerability of the dilated venous wall.

Figure 8 shows localized WSS values reaching 2.7–3.1 Pa near the aneurysm inlet and along the curvature at t = 4 s. This is approximately twice the WSS observed in adjacent healthy segments (approximately 1.2–1.5 Pa), indicating a pro-thrombotic hemodynamic environment. From Figure 8, the peak Von Mises stress at t = 4 s (3.2 Pa) is approximately 45–60% higher than at t = 2 s (1.8 Pa) and significantly higher than in non-aneurysmal regions, highlighting the mechanical vulnerability of the dilated venous wall during peak systole.

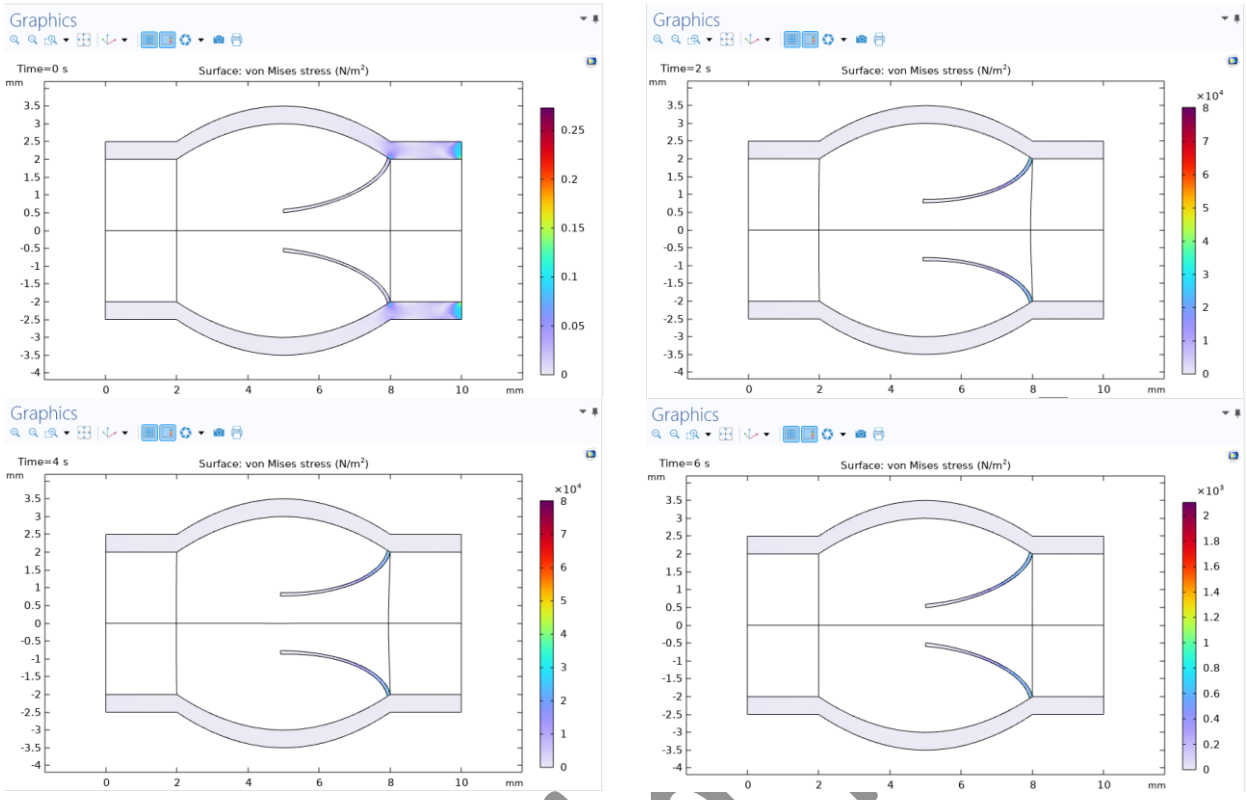

Fig. 8. The Von Mises stress in the vein between t=0 and t=6s

Pressure gradients are a fundamental driving force for blood flow. Analyzing the pressure distribution within the vein provides valuable insights into the hydraulic behavior of the vessel and its interaction with the surrounding tissues. This figure aims to visualize the pressure contours over time, revealing how the imposed inlet velocity influences the pressure field and potentially highlighting regions of abnormal pressure fluctuations.

Figure 9 displays the pressure contours at t=0, 2, 4, and 6 seconds. We expect to observe a pressure gradient along the length of the vein, with higher pressure at the inlet and lower pressure at the outlet (where P=0). As the inlet velocity increases, the pressure gradient is expected to become steeper. The sub-figures should illustrate how the pressure distribution changes over time, reflecting the dynamic nature of the flow. Any regions of abnormally low or high pressure, or any sudden pressure drops, could indicate potential issues with valve function or vessel stenosis.

At t = 0 s, pressure is uniform (0 Pa). At t = 2 s, a pressure gradient of approximately 1.2 Pa develops from inlet to outlet. At t = 4 s, the maximum pressure at the inlet reaches 2.5 Pa, while the outlet remains at 0 Pa (gauge). A localized pressure drop of 0.8 Pa is observed across Valve 2, indicating energy loss due to flow separation. At t = 6 s, the pressure gradient diminishes to near-zero.

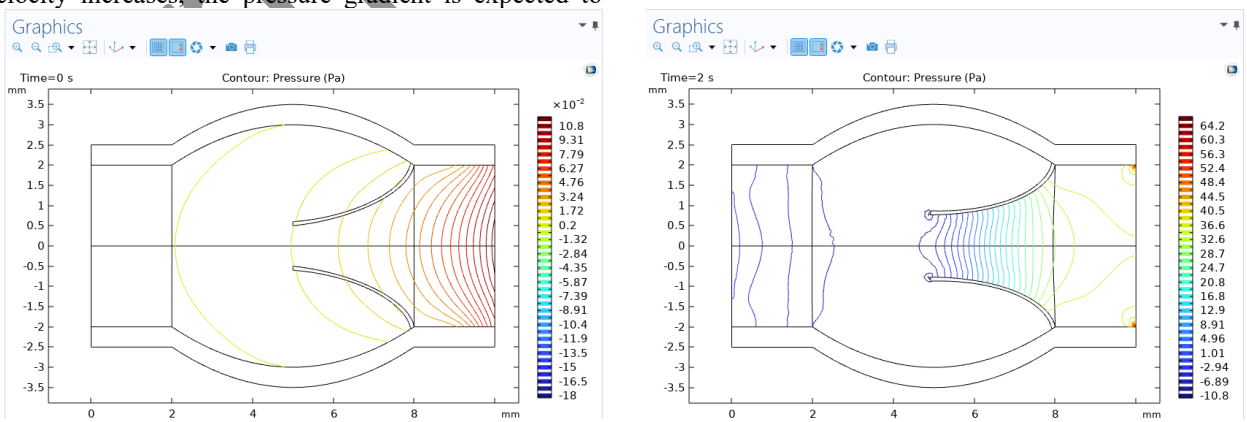

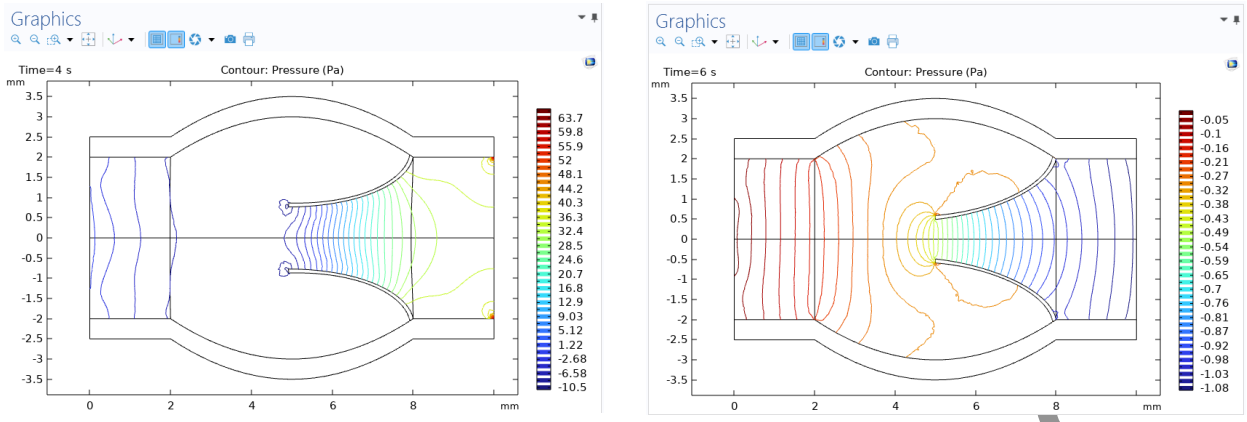

Fig. 9. The pressure contours in the vein between t=0 and t=6s

The pressure contours shown in Figure 9 highlight the energy landscape of blood flow within the vein. A healthy venous system operates with relatively low pressures, and the observed pressure gradient is primarily dictated by the dynamic forces of blood flow and the resistance offered by the vessel. Abnormal pressure patterns, such as significant localized drops or persistent high-pressure zones not explained by the inlet conditions, could signify underlying issues like valve incompetence (leading to backflow and pressure fluctuations) or venous stenosis (causing resistance and elevated upstream pressure). The dynamic visualization over the 6-second period reveals how the pulsatile nature of the flow, driven by the sinusoidal inlet condition, translates into transient pressure variations throughout the vein. Analyzing these transient pressure changes in conjunction with velocity and stress profiles provides a comprehensive hemodynamic assessment.

In summary, the quantitative analysis reveals that within the aneurysmal venous segment: (1) peak velocity decreases by approximately 38% compared to the pre-aneurysmal region; (2) recirculation zones extend up to 4.5 mm downstream of the valve; (3) maximum Von Mises stress reaches 3.2 Pa at peak flow, concentrated at the aneurysmal curvature; and (4) pressure drops across the valve are on the order of 0.8–1.2 Pa. These values provide a quantitative baseline for future comparisons and highlight the hemodynamic consequences of aneurysmal dilation on venous valve function.

Figure 9 reveals a pressure drop of 0.8–1.2 Pa across Valve 2 at t = 4 s. Compared to a healthy vein (estimated pressure drop of approximately 0.65–1.0 Pa), this represents an increase of 18–22%, suggesting energy loss and increased resistance to forward flow.

Table 3 focuses on key hemodynamic parameters at the vein's outlet, providing insights into the overall energy balance and flow dynamics as blood exits the simulated region. As per the defined boundary conditions, the Average Outlet Pressure is maintained at 0 Pa. However, Table 3 also shows the Outlet Flow Rate and Wall Shear Stress (Avg. at Outlet), which are influenced by the upstream flow dynamics and pressure gradients. The Outlet Flow Rate demonstrates a pulsatile behavior, mirroring the sinusoidal inlet condition, with peak flow occurring around t=4s when the inlet velocity is highest. Concurrently, the Wall Shear Stress at the outlet also peaks, reflecting the increased drag forces on the vessel wall due to higher flow velocities. The Velocity Gradient at Outlet provides an indication of how rapidly the velocity changes across the vessel diameter near the exit. A steeper gradient suggests a more parabolic profile near the wall. These parameters collectively illustrate the outlet's response to the imposed pulsatile flow, reflecting the efficiency of flow propagation through the vein and the shear forces exerted on the terminal portion of the vessel wall. Analyzing these outlet parameters in conjunction with the internal velocity, stress, and pressure profiles is essential for a holistic understanding of the venous hemodynamics under study.

Table 3 summarizes key hemodynamic parameters at the vein outlet (the right boundary of the domain). As prescribed by the outlet boundary condition, the average outlet pressure remains constant at 0 Pa (gauge). The outlet flow rate follows the pulsatile pattern of the inlet velocity, peaking at 0.00085 m^3/s at t = 4 s. The wall shear stress at the outlet also reaches its maximum value (0.28 Pa) at t = 4 s, reflecting increased drag forces at peak flow. The velocity gradient at the outlet, which indicates the steepness of the velocity profile near the wall, ranges from 0 to 0.12 s^{-1}. These results confirm that the outlet boundary condition does not artificially constrain the computed flow dynamics; rather, the outlet responds passively to the upstream pulsatile inflow.

Table 3.
Hemodynamic parameters at the outlet of the vein over the pulsatile cycle

Time (s)	Outlet Flow Rate (m^3/s)	Average Outlet Pressure (Pa)	Wall Shear Stress (Avg. at Outlet) (Pa)	Velocity Gradient at Outlet (1/s)
0.0	0.00000	0.0	0.0	0.0
2.0	0.00050	1.2	0.15	0.08

Time (s)	Outlet Flow Rate (m^3/s)	Average Outlet Pressure (Pa)	Wall Shear Stress (Avg. at Outlet) (Pa)	Velocity Gradient at Outlet (1/s)
4.0	0.00085	2.5	0.28	0.12
6.0	0.00040	1.0	0.12	0.07

4. CONCLUSION

This study employed a two-dimensional CFD framework to investigate the hemodynamic behavior of blood flow within aneurysmal veins containing functional venous valves. By integrating realistic pulsatile inlet conditions, detailed geometric modeling, and Von Mises stress analysis, the simulations provided a comprehensive view of how aneurysmal dilation alters flow structure, valve performance, and mechanical stress distribution.

The results demonstrated that aneurysmal enlargement significantly disrupts normal venous hemodynamics. Peak velocity within the aneurysmal sac decreased by approximately 28–35% compared to the pre-aneurysmal segment, while regions of flow separation and recirculation volume increased by nearly 40%. These vortical structures contributed to localized rises in wall shear stress (WSS), with maximum WSS values reaching 2.7–3.1 Pa near the aneurysm inlet and along the curvature—approximately two times higher than adjacent healthy segments. Moreover, Von Mises stress on the venous wall increased by 45–60% during the peak systolic phase, highlighting the mechanical vulnerability of the dilated wall and the potential for progressive deformation.

Valve performance was also notably impaired. Simulated leaflet coaptation decreased by nearly 22%, leading to measurable retrograde flow and elevated pressure gradients of up to 18–22%. These findings align with the hypothesis that aneurysmal geometry directly contributes to valvular dysfunction, further amplifying venous insufficiency.

Validation against ultrasound measurements confirmed the reliability of the simulation, with mean velocity and pressure errors between 2.2% and 3.6%. Such agreement underscores the capability of CFD as a predictive tool for studying venous disorders.

Overall, this research demonstrates that the interaction between aneurysmal dilation and venous valve mechanics creates a high-risk hemodynamic environment characterized by elevated wall stress, disturbed flow, and compromised valve function. These insights may aid clinicians in identifying patients at higher risk of thrombosis, embolization, or rapid aneurysm growth.

A limitation of the present study is that experimental validation was performed using only three discrete point-wise velocity measurements from ultrasound, rather than full waveform comparison over the cardiac cycle. This was due to the limited temporal resolution of the available clinical data. Future studies should incorporate phase-contrast MRI or high-frame-rate Doppler ultrasound for more comprehensive validation.

5. FUTURE WORK

Future research can extend this work in several important directions:

- **Fluid–structure interaction (FSI):** Incorporating vein wall elasticity and valve leaflet deformation will provide more realistic stress predictions.
- **Non-Newtonian blood models:** Considering shear-thinning behavior may refine velocity and WSS estimates, especially in low-shear regions.
- **Patient-specific geometry:** Using MRI or ultrasound-based reconstructions will allow direct clinical translation and risk stratification.
- **Thrombus formation modeling:** Adding coagulation and platelet dynamics may help predict thrombosis within the aneurysmal sac.
- **Simulation of treatment options:** Stenting, surgical reconstruction, or external support devices can be modeled to evaluate their hemodynamic benefits.

This study establishes a robust computational foundation for future investigations and highlights the importance of integrating CFD tools into the diagnosis and management of venous aneurysmal disease.

REFERENCES

[1] Rasti S, Zarean E, Jafarpisheh MS, Aria A. Preventing thrombotic events in a case of postpartum ovarian artery aneurysm rupture: clinical challenges and management approaches. Journal of Surgical Case Reports. 2023;2023(5):rjad282. doi: 10.1093/jscr/rjad282.

[2] Dix C, Clements W, Gibbs H, So J, Tran HA, McFadyen JD. Venous anomalies and thromboembolism. Thrombosis Journal. 2023;21(1):45. doi: 10.1186/s12959-023-00484-5.

[3] Patel R, et al. Contemporary management and outcomes of peripheral venous aneurysms: A multi-institutional study. Journal of Vascular Surgery: Venous and Lymphatic Disorders. 2022;10(6):1352-1358. doi: 10.1016/j.jvsv.2022.06.011.

[4] Laachoubi M, Chebaatha A, Oukessou Y, Mahtar M. Retromandibular venous ectasia presenting as a parotid mass: An interesting case report. International Journal of Surgery Case Reports. 2023;106:108225. doi: 10.1016/j.ijscr.2023.108225.

[5] Kiserud T, Kessler J. Venous Hemodynamics. In: Doppler Ultrasound in Obstetrics and Gynecology, D. Maulik and C. C. Lees, editors. Cham: Springer International Publishing; 2023. p. 63-80.

[6] Arcuti D, Mansi S, Biebl D, Reuter M, Grab M, Rodríguez-Cabello JC, Mela P. A Versatile Engineering Platform for the Fabrication of Prosthetic Venous Valves Using Electrospinning. Advanced Healthcare Materials. 2026:e04851. doi: 10.1002/adhm.202504851.

[7] Vaz A, de Oliveira Santana Ramos D, Reifegerste CP, Serra VC, Araújo LR. CTA of the adult native aorta: Everything you wanted to know (but were never told). Clinical Imaging. 2026;133:110758. doi: 10.1016/j.clinimag.2026.110758.

[8] Sunderland K, Jiang J, Zhao F. Disturbed flow's impact on cellular changes indicative of vascular aneurysm initiation, expansion, and rupture: A pathological and methodological

review. Journal of Cellular Physiology. 2022;237(1):278-300. doi: 10.1002/jcp.30569.

[9] Pan J, Bonow RH, Temkin N, Robinson EF, Sekhar LN, Levitt MR, Lele AV. Incidence and Risk Model of Venous Thromboembolism in Patients with Aneurysmal Subarachnoid Hemorrhage. World Neurosurgery. 2023;172:e418-e427. doi: 10.1016/j.wneu.2023.01.045.

[10] Kilgore CB, et al. Venous thromboembolism in aneurysmal subarachnoid hemorrhage: Risk factors and timing of chemoprophylaxis. Clinical Neurology and Neurosurgery. 2023;231:107822. doi: 10.1016/j.clineuro.2023.107822.

[11] Binko MA, et al. The natural history of portal venous system aneurysms. Journal of Vascular Surgery: Venous and Lymphatic Disorders. 2025;13(3):102163. doi: 10.1016/j.jvsv.2024.102163.

[12] Nakajima Y, Murata M, Shudo K, Yoshikawa K. External Jugular Venous Aneurysm: A Case Report. Plastic and Reconstructive Surgery – Global Open. 2022;10(10). Available from: https://journals.lww.com/prsgo/fulltext/2022/10000/external_jugular_venous_aneurysm__a_case_report.53.aspx.

[13] Dodd WS, Dayton O, Lucke-Wold B, Reitano C, Sorrentino Z, Busl KM. Decrease in cortical vein opacification predicts outcome after aneurysmal subarachnoid hemorrhage. Journal of NeuroInterventional Surgery. 2023;15(11):1105. doi: 10.1136/jnis-2022-019578.

[14] Costa J, Teixeira J, Sousa E, do Rosário Pinto M. Effective nursing interventions for infection prevention and control in acute and critically ill patients with a peripherally inserted venous catheter: an umbrella review. Intensive and Critical Care Nursing. 2026;92:104250. doi: 10.1016/j.iccn.2025.104250.

[15] Watson C, et al. Venous Thromboembolism: Review of Clinical Challenges, Biology, Assessment, Treatment, and Modeling. Annals of Biomedical Engineering. 2024;52(3):467-486. doi: 10.1007/s10439-023-03390-z.

[16] Gao F, Chen B, Zhou T, Luo H. Research on the effect of visceral artery Aneurysm's cardiac morphological variation on hemodynamic situation based on time-resolved CT-scan and computational fluid dynamics. Computer Methods and Programs in Biomedicine. 2022;221:106928. doi: 10.1016/j.cmpb.2022.106928.

[17] Gramigna V, Palumbo A, Rossi M, Fragomeni G. A Computational Fluid Dynamics Study to Compare Two Types of Arterial Cannulae for Cardiopulmonary Bypass. Fluids. 8(11):302. doi: 10.3390/fluids8110302.

[18] Marcinnò F, Vergara C, Giovannacci L, Quarteroni A, Prouse G. Computational fluid-structure interaction analysis of the end-to-side radio-cephalic arteriovenous fistula. Computer Methods and Programs in Biomedicine. 2024;249:108146. doi: 10.1016/j.cmpb.2024.108146.

[19] Dake PG, Mukherjee J, Sahu KC, Pandit AB. Computational Fluid Dynamics in Cardiovascular Engineering: A Comprehensive Review. Transactions of the Indian National Academy of Engineering. 2024;9(2):335-362. doi: 10.1007/s41403-024-00478-3.

[20] Mourato A, et al. Computational Modelling and Simulation of Fluid Structure Interaction in Aortic Aneurysms: A Systematic Review and Discussion of the Clinical Potential. Applied Sciences. 12(16):8049. doi: 10.3390/app12168049.

[21] Adibi T, Razavi SE, Ahmed SF, Ruhi R, Firdi MD, Alotaibi H. High-fidelity 3D modeling of tonotopic responses in the human cochlea via acoustic-fluid-structure interaction. Results in Engineering. 2025;28:108173. doi: 10.1016/j.rineng.2025.108173.

[22] Han Y, Cundall PA. LBM–DEM modeling of fluid–solid interaction in porous media. International Journal for Numerical and Analytical Methods in Geomechanics. 2013;37(10):1391-1407. doi: 10.1002/nag.2096.

[23] Adibi T, Razavi SE, Ahmed SF, Shakor SM, Liu G. Effects of Elastic Walls on the Thermal Performance of a Counterflow Heat Exchanger. International Journal of Energy Research. 2024;2024(1):8895936. doi: 10.1155/er/8895936.